Part I of II

Technical Strategies for Voltage Power Regulation in LV Distribution Networks

Maurizio Delfanti, Luisa Frosio, Gabriele Monfredini, Marco Merlo, Claudio Rosati, Daniele Rosati, and Gabriele Marchegiani

ABSTRACT

We report the integration of a novel voltage regulation strategy in the inverter control algorithm for Dispersed Generation (DG) applications. The adoption of a decentralized voltage control based on local curves allows the voltage profile to be controlled at the Point of Common Coupling (PCC) of the generators and, therefore, the capacity of existing distribution networks to host more generation from renewables. The work is focused on a low voltage distribution network and both the reactive power modulation and the real power curtailment are considered in the proposed local strategy. Both numerical and experimental analysis are necessary in order to test and validate the proposed voltage control strategy. Firstly, the performances of the proposed control are tested by a numeral analysis and the impact on both the electrical system and the inverter apparatus is evaluated. Secondly, the benefit of the control strategy is analysed by experimental analysis in a test facility to verify the feasibility of voltage regulation in a real feeder.

Keywords: Dispersed Generation, over-voltage, voltage regulation, inverter control, point of common coupling

INTRODUCTION

In the past, distribution networks were designed to be passive systems, i.e. without Dispersed Generation (DG) connected. Until recently, DG units were managed according to the fit and forget approach: in compliance with the standard of European countries they operate without providing any service to the distribution system, but just supplying energy to the network according to the availability of the primary energy source.

The fast increase of DG power injections at Medium Voltage (MV) and Low Voltage (LV) level affect power flows along distribution feeders: in particular a reverse power flow can occur along the radial feeder and the voltage profile is no longer monotonous. As a consequence, over-voltages at the DG Point of Common Coupling (PCC) can occur (i.e. violation of EN 50160 prescriptions [1]).

Therefore, the impact on the electrical distribution system is significant; the current voltage systems are intended for passive networks and they are not able to guarantee a reliable voltage quality level with high penetration of DG. Generally, the On-Load Tap Changer (OLTC) is set up in the Primary Substation (PS) and it operates locally reading the voltage at the MV busbar of the PS; moreover, by means of the load drop compensator, the voltage set-point can be modified to compensate the effect of the load [3].

DG injections at distribution level alter the power flow in the HV/MV transformer (i.e. decreasing the load compensation); thus, voltage regulation that acts only through substation level measurements is not sufficient to maintain voltage within the constraints in all busses of the network, but mainly in peripheral busses of the network and where the DG is connected.

Several proposals have been put forward in the literature on the matter: [4] and [5] focus on performing regulation structure, but real time measures about load consumptions and generation injections are necessary and state estimation techniques are required.

As DG penetration increases it will become a technical and economic imperative that DG participates in the provision of ancillary services needed for a secure and reliable operation of the power system. This is important for the simple reason that if DG only displaces the energy produced by central generation but not the associated flexibility and capacity, the overall cost to operate the entire system will rise. To have a more effective voltage regulation it is necessary to exploit DG units as voltage control resources (or, practically, as reactive power resources). In this way DG is a decentralized voltage regulation resource in the distribution network [6].

This article proposes a new local voltage control strategy to be integrated in the inverter of DG units connected to the LV grid. In particular, DG's reactive power is modulated according to local measurements at the DG PCC. Beside the reactive power modulation service, as back-up solution a real power curtailment can be also adopted in order to mitigate high power injections affecting the voltage profile.

The modulation of reactive power together with a real power injection introduces a leading/lagging component of the current and an in-

crease in the RMS value. Possible loss deterioration in the inverter system can occur due to the reactive power modulation.

The experimental activity was carried out in cooperation with MCM Energy Lab srl for the system set up and the software development, and with ELVI Spa, who provided the PV inverters and the test facility.

This report is organised as follows: first the impact of the DG in the LV distribution network is analysed; then, local voltage control laws, which exploit DG units as control resources, are introduced with the goal to improve voltage quality, moreover, two real power curtailment logics are presented. Next, the inverter system update required for the reactive power regulation is discussed and the details about the new inverter control is given. Then, a numerical analysis is described to test the impact of the local control strategies on the distribution system. Furthermore, the effect of the reactive power modulation on the inverter system is evaluated. Next, an experimental application of a multi-inverter configuration is proposed. Finally, the conclusions and remarks of the work are presented.

IMPACT OF DG ON THE LV DISTRIBUTION NETWORK

Referring to the EU standard, the voltage limits in the LV distribution system are ±10% of the rated voltage Un for 95% of the time, and +10/-15% always (EN 50160 [1]; the voltage has to be intended as the mean r.m.s. value computed in a 10-minute period).

In a passive network (no DG connected) the voltage profile decreases monotonously along the feeder. If DG units are connected, the voltage profile may no longer be monotonous.

According to the power mismatch between load and generation, DG can lead to serious over-voltages to other connected customers or contribute to sustaining the feeder voltage profile. Indeed, the coordination of transformer tap in PS and SS becomes difficult to achieve. It is reasonable to claim that the higher the R/X ratio the higher the impact of the real power on the voltage. The LV distribution system is made up of cable with small cross-section, therefore such networks are characterised by a high R/X ratio that makes voltage increase a particular problem [20] [21].

Recently, voltage issues have emerged in LV networks because of the large expansion of distributed photovoltaic generations [9]. In fact, the total PV installed power in 2012 in the Italian LV distribution system was 5085 MW and the number of power plants installed was 458265 (i.e.

an average size of 11 kW per power plant) [10]. The PV system represents almost all the DG connected to the LV system. Generally, because of the existing regulations on distribution networks (in Italy, [11]) DSO is compelled to accept all DG connection requests.

Thus, to manage the voltage profile of a distribution network, a viable solution could be based on DG reactive power injections modulation. This is being assessed in several countries. Voltage control can be attained adopting a local-corrective control strategy, achievable with reduced investments. According to the Italian standard CEI 0-21 [14] DSO could impose voltage regulation on active users connected to the LV network. This standard suggests two control solutions in which the reactive power is modulated according to local measurements of either voltage or real power injected. Recently, the Italian standard CEI 0-16 [17] extended the same local control strategies to the MV distribution system. Similarly, in the latest German technical guideline for LV networks rules are provided for generator connection and two reactive power provisions are given, which are the fixed power factor method and the power factor as a function of the real power generation method [18]. In France, ERDF investigates the reactive power management of DG following a dynamic regulation law; the regulation mode for reactive power management is discussed among three approaches: fixed reactive power, reactive power modulation as a function of the real power and according to a characteristic [19].

This paper aims to evaluate the effectiveness of the local control strategies on the voltage profile enhancement in the LV distribution system and a comparison of the different curves is performed. In particular, a numerical analysis is conducted in order to simulate the effectiveness of the reactive power modulation in the voltage control in an LV system. Afterwards, an experimental analysis is carried out in a real LV test network in order to test the feasibility of the voltage control solutions proposed and the stability of the regulation in a multi-generation scenario.

Since LV cables are characterised by high resistance parameter values, it could be necessary to absorb a significant amount of reactive power to bring back voltage within the voltage limits. The high R/X ratio of LV lines limits the effectiveness of a regulation based on reactive power modulation; on the contrary, a real power curtailment will be quite effective on the voltage profile [15][16]. Voltage violations could be eliminated paying a reduction of DG power injection with respect to the energy theoretically available (i.e. lack of profit for the energy producer viewpoint). The first curtailment technique proposed is a DG disconnection by means of the

IPS (Interface Protection System) when the upper-voltage limit is reached, whereas the second curtailment strategy, named DG limitation, only limits the DG injections until the voltage goes back within its limit. In this paper the advantage of the combined effect of reactive power modulation and real power curtailment is analysed by exploiting numerical analysis.

LOCAL VOLTAGE CONTROL STRATEGIES

According to the voltage issues described in the previous paragraph, the paper aims to analyse the performances of a decentralized voltage control strategy that exploits DG units as reactive power resources.

In the local control each generator operates locally without coordination to other devices; it is a simple strategy, easy to implement and it does not require a communication infrastructure (no investment in network assets) [7]. In this work four local control laws have been investigated; they summarize the laws proposed in the European technical standards.

Generally, the reactive modulation is based on local measurements available at PCC of the generator (voltage or real power injections). Local control strategies could be classified w.r.t. the variables monitored:

Law A. $tg\phi = f(u)$, control of tangent of ϕ according to the PCC voltage;
Law B. $q = f(u)$, control of reactive power according to the PCC voltage;
Law C. $tg\phi = f(p)$, control of tangent of ϕ according to the real power injected;
Law D. $q = f(p)$, control of reactive power according to the real power injected.

The first possible solution (Law A) is depicted in Fig. 1. This method involves two conditions: a normal operating situation, where no control action is required, and a situation where first voltage thresholds (*u1* and *u2*) are violated. In the latter case the generator operates at $tg\phi$ different from zero according to the local voltage. The reactive power injected/absorbed from the network depends on the real power injected p according to the formula $q = p \cdot tg\phi$, therefore it is determined by both the voltage and the real power injections. By adopting this strategy it is possible to have a significant impact on the voltage profile only when the DG unit injects a real power amount close to the rated value.

According to the network response, the DG unit operates in a specific working point of the $tg\varphi$-u domain: it is the intersection between the

local control curve and the reactive characteristic of the network.

The second solution proposed (Law B, Fig. 2) is similar to the previous one, but the reactive power is directly modulated according to the voltage measured at PCC irrespective of the real power production. By this strategy the DG unit can operate, in the case of low real power injections, at a power factor lower than the one imposed by Law A. Higher reactive power modulation involved in this strategy causes a higher stress on generators for the mitigation of the over-voltages in the network.

The two characteristics described above operate according to the local voltage measurements; the voltage feedback allows involving the requested amount of reactive power for voltage mitigations until the power plant reaches its reactive power limits.

Furthermore, the proposed voltage control limits the regulation actions of generators only when the nodal voltage exceeds a pre-defined range. In this way, the reactive power generated by the DG is null when the network voltage is within acceptable levels, limiting the current flow and avoiding real power loss increases.

The last two local control strategies proposed, Law C and Law D, act directly according to the real power injected by the DG. The effectiveness of these characteristics is based on the fact that power flows from the DG plants to the secondary substation are directly responsible for voltage increase at the PCC. Therefore, in the case of large amounts of DG it is appropriate to involve reactive power in order to mitigate the over-voltages.

Law C is shown in Fig. 3. The value of tangent of ϕ is modulated according to the real power injected by the generator. Especially, in the case of higher injections than a predefined threshold *p1* the control tries to reduce the voltage rise lagging reactive power from the grid (i.e. working at negative $tg\phi$). This strategy can be achieved as follows:

- without taking into account the voltage at the PCC (as proposed by VDE [18]),
- with a voltage lock-in that triggers the regulation and, in the same manner, with a voltage lock-out that allows the control deactivation in case of low voltages (as proposed by the Italian regulation [14]).

Finally, the last solution proposed, Law D, is similar to the previous one, but the only difference is that control is achieved by directly modulating the reactive power, in compliance with the regulation curve reported in Fig. 4. The parameters of the voltage control laws adopted in the simulations are reported in Tables 1 and 2.

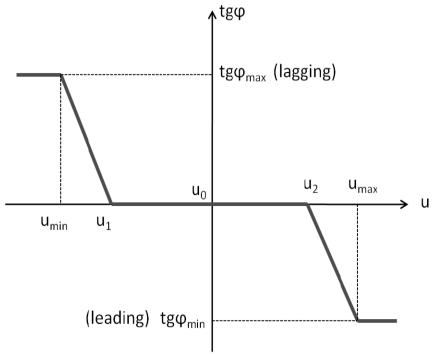

Fig. 1: Local voltage control strategy $tg\phi = f(u)$ (Law A)

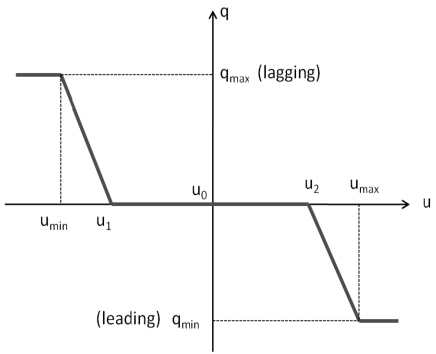

Fig. 2: Local voltage control strategy $q = f(u)$ (Law B)

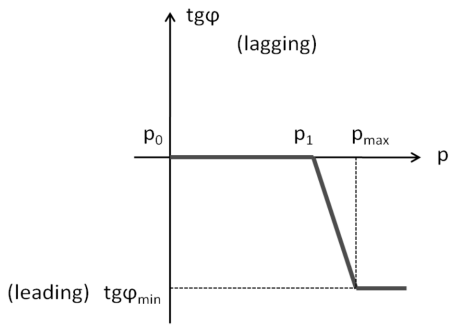

Fig. 3: Local voltage control strategy $tg\phi = f(p)$ (Law C)

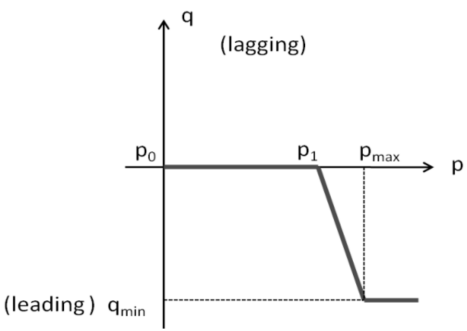

Fig. 4: Local voltage control strategy $q = f(p)$ (Law D)

Table 1: Control law parameters—Law A and Law B

	Law A	Law B
$u_0[p.u.]$	1	1
$u_1[p.u.]$	0.95	0.95
$u_2[p.u.]$	1.05	1.05
$u_{\max}[p.u.]$	1.1	1.1
$u_{\min}[p.u.]$	0.9	0.9
$tg\phi_{\max}$	0.4843	/
$tg\phi_{\min}$	-0.4843	/

Table 2: Control law parameters—Law C and Law D

	Law C	Law D
$p_0[p.u.]$	0	0
$p_1[p.u.]$	0.5	0.5
$p_{\max}[p.u.]$	0.9	0.9
$tg\phi_{\min}$	-0.4843	/
$q_{\min}[p.u.]$	/	-0.4359
$Lock-in[p.u.]$	1.05	1.05
$Lock-out[p.u.]$	0.98	0.98

INVERTER SYSTEM MODEL UPDATE FOR REACTIVE POWER REGULATION

In order to evaluate the practicability of the local voltage control proposed in the previous chapter, it is important to investigate the effect of the reactive power modulation on the converter machine in terms of operational performances and losses. Recently the inverters for DG application have been controlled to operate only at unitary power factor and no reactive power flow is involved. On the contrary, an upgrade of the inverter algorithm is necessary to guarantee the implementation of the voltage regulation [22].

The inverter adopted for PhotoVoltaic (PV) applications is basically a single stage DC-AC three-phase converter connected to the AC network through a 270/400 V step up transformer; the voltage at the DC-Link is usually kept in the range between 450 V and 800 V directly through the PV field by means of a DC/DC boost converter. The functional scheme of the inverter system is reported in Fig. 5. This devise provides an interface to the PV system for real and reactive power exchange with the AC grid. A common commutation technique adopted for the inverter is the space vector and the converter can be modelled as a DC-voltage controlled AC-voltage source.

The block diagram of a generic inverter control adapted for the reactive power control is reported in Fig. 6. The AC voltage phasor upstream the transformer $V_{grid270}$ is controlled by the "Inverter Modulator" block that generates the gates for the IGBT of the inverter [25]. A d-q rotating reference-system synchronous with at the AC voltage phasor $V_{grid270}$ is

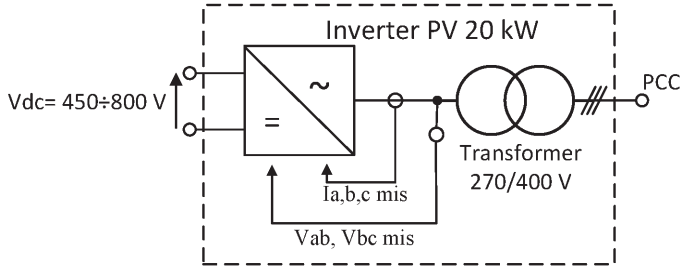

Fig. 5: Inverter functional pattern

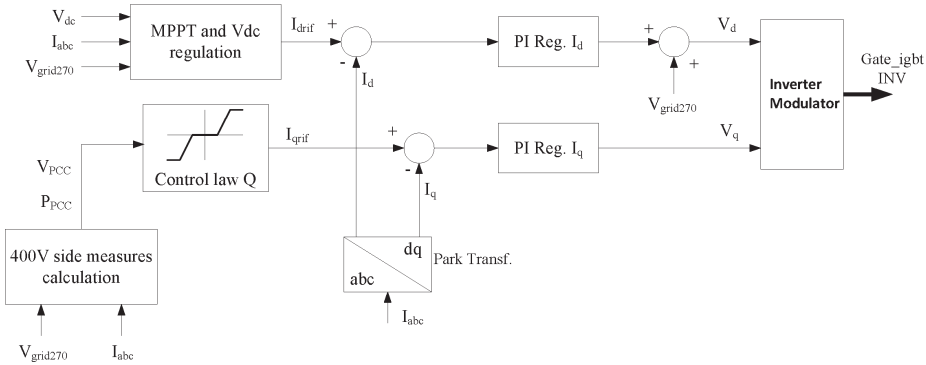

Fig. 6: Block diagram of the adapted control algorithm for the reactive power control

introduced to decouple the control of the real and reactive power of the inverter by means of the current components *Id* and *Iq* respectively (as detailed in [30] and [23]).

Nowadays, the control algorithm of PV inverters, in both MV and LV systems, controls the real power injection to achieve the Maximum Power Point Tracker (MPPT) of the photovoltaic modules and a reactive power control is not implemented (Iqrif = 0).

In order to ensure the reactive power modulation the following additional functions have to be set up [24]:

Function 1: control of the Iq component of the AC output current, in order to follow the local control law,

Function 2: control of the voltage at the DC-Link in order to maintain a stable operation even in the case of lack of the primary source and to avoid reverse power flow toward the photovoltaic panels,

Function 3: the pre-charge function at the DC bus.

Functions 2 and 3 allow the capacitor to be pre-charged at the DC-Link by absorbing energy from the AC network. These functions are required to control the reactive power even if the real power injection is zero (necessary for the control strategy Law B). Functions 1 and 2 require only an update of the software algorithm of the inverter to achieve the control of the q-axes current and the DC-Link voltage respectively. Conversely, function 3 needs a hardware update for the introduction of the pre-charge circuit, in order to absorb energy directly from the grid, and a software update in order to manage the pre-charge which is created when the DC-Link capacitor is discharged and the primary source is not present.

Basically, function 1 is achieved by modifying the algorithm of the inverter control. Figure 6 shows the complete control scheme of the inverter that includes the update required for the control of the reactive current component. As in a standard control, the I_{drif} value is defined by the "MPPT and Vdc regulation" block in order to fix the voltage of the DC-Link at a suitable value according to the MPPT algorithm.

According to the update of function 1. the reactive power injected at the AC side is controlled by defining the setpoint I_{drif} of the lagging current component. The I_{drif}value is defined according to one of the control laws described in paragraph 0. The four local voltage laws are set up in the block "Control law Q" of the control frame: according to the values of the PCC voltage V_{PCC} or the PCC real power P_{PCC}, the reference current I_{drif} that corresponds to a defined amount of reactive power is generated. Two PI regulators define the voltage references Vd and Vq independently as a function of the d and q current errors.

As shown in Fig. 5, actually inverter measurements are related to the 270 V AC side of the transformer but, in order to implement the control laws at the PCC, the measurements at the 400 V site are needed. For this reason, the software of the control algorithm needs to be adapted to estimate the voltage and the real power measurements downstream of the transformer. The estimation of the PCC measurements is achieved by compensating the effects of both the voltage drop and power losses of the boost transformer. For this purpose the new block "400V side measures calculation" is introduced in the block diagram (as shown in Fig. 6).

The voltage at the PCC VPCC can be computed starting from the voltage measured at the 270 V side of the transformer VMEA by the following formula in which the VPCC is considered on the d-axis:

10% Online Discount Use Code JR10

Energy Resilient Buildings & Communities: A Practical Guide

Brian Levite and Alexander Rakow

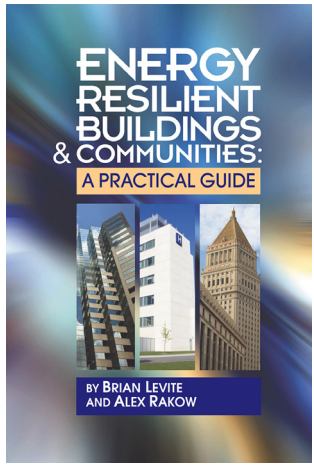

This book is written as a practical guide to those interested in the pursuit of energy resilience at a local scale. Energy resilience is defined as the relative ability of an institution to carry out its mission during a shock to the energy system, and to approach the concept on the level of a single site occupied by a single community or institution. Examples are drawn from four key community types: military bases, healthcare campuses, educational campuses and municipal governments. The book then describes a framework for developing an energy resilience plan that applies to each. While the focus is clearly on the U.S., understanding the energy resilience threat and conducting long-range energy resilience planning will benefit communities all over the globe. Part I describes the specific energy security threats that are facing local institutions and communities, the specific impact of an energy shock, and the advantages offered by pursuit of energy resilience. Part II provides concrete guidance and allows managers to assess where their institution lies on the energy resilience spectrum and they would like to be. Part III describes the three main areas of energy resilience performance: energy efficiency, on-site generation, and emergency planning. Case studies are also provided.

ISBN0-88173-718-6

6 x 9, 214 pp, Hardcover
$110

Order Code 0705

CONTENTS

BOOK ORDER FORM

① Complete quantity and amount due for each book you wish to order:

Quantity	Book Title	Order Code	Price	Amount Due
	Energy Resilient Buildings & Communities: A Practical Guide	**0705**	**$110.00**	

② Indicate shipping address: CODE: Journal 2015

NAME (Please print) BUSINESS PHONE

SIGNATURE (Required to process order) EMAIL ADDRESS

COMPANY

STREET ADDRESS ONLY (No P.O. Box)

CITY, STATE, ZIP

Applicable Discount	
Georgia Residents add 6% Sales Tax	
Shipping $10 first book $4 each additional book	**10.00**
TOTAL	

MEMBER DISCOUNTS—A 15% discount is allowed to AEE members (discounts cannot be combined).
☐ **AEE Member (Member No._____)**

③ Select method of payment:
☐ **CHECK ENCLOSED**
☐ **CHARGE TO MY CREDIT CARD**
☐ *VISA* ☐ *MASTERCARD* ☐ *AMERICAN EXPRESS*

Make check payable in U.S. funds to: **AEE ENERGY BOOKS**

CARD NO.

Expiration date *Signature*

④ Send your order to:
AEE BOOKS
P.O. Box 1026
Lilburn, GA 30048

INTERNET ORDERING
www.aeecenter.org/books
(use discount code)

TO ORDER BY PHONE
Use your credit card and call:
(770) 925-9558

TO ORDER BY FAX
Complete and Fax to:
(770) 381-9865

INTERNATIONAL ORDERS
Must be prepaid in U.S. dollars and must include an additional charge of $10.00 per book plus 15% for shipping and handling by surface mail.

10% Online Discount Use Code JR10

AUTOMATED DIAGNOSTICS AND ANALYTICS FOR BUILDINGS

Edited by Barney L. Capehart, Ph.D., and Michael R. Brambley, Ph.D.

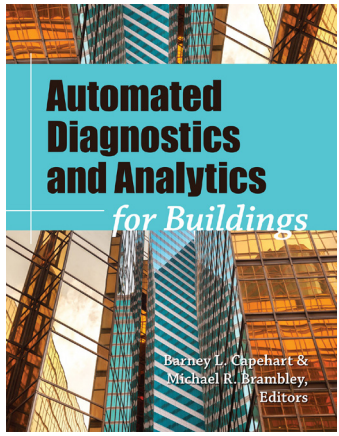

With the widespread availability of high-speed, high capacity microprocessors and microcomputers with high-speed communication ability, and sophisticated energy analytics software, the technology to support deployment of automated diagnostics is now available, and the opportunity to apply automated fault detection and diagnostics to every system and piece of equipment in a facility, as well as for whole buildings, is imminent. The purpose of this book is to share information with a broad audience on the state of automated fault detection and diagnostics for buildings applications, the benefits of those applications, emerging diagnostic technology, examples of field deployments, the relationship to codes and standards, automated diagnostic tools presently available, guidance on how to use automated diagnostics, and related issues.

ISBN: 0-88173-732-1

8½ x 11, 615 pp., Illus.
Hardcover

$175
Order Code 0695

CONTENTS

BOOK ORDER FORM

① Complete quantity and amount due for each book you wish to order:

Quantity	Book Title	Order Code	Price	Amount Due
	Automated Diagnostics and Analytics for Buildings	**0695**	**$175.00**	

② Indicate shipping address: CODE: Journal 2014

NAME (Please print) BUSINESS PHONE

SIGNATURE (Required to process order) EMAIL ADDRESS

COMPANY

STREET ADDRESS ONLY (No P.O. Box)

CITY, STATE, ZIP

Applicable Discount	
Georgia Residents add 6% Sales Tax	
Shipping $10 first book $4 each additional book	**10.00**
TOTAL	

MEMBER DISCOUNTS—A 15% discount is allowed to AEE members (discounts cannot be combined).
☐ **AEE Member (Member No._____)**

③ Select method of payment:
☐ **CHECK ENCLOSED**
☐ **CHARGE TO MY CREDIT CARD**
☐ *VISA* ☐ *MASTERCARD* ☐ *AMERICAN EXPRESS*

Make check payable in U.S. funds to: **AEE ENERGY BOOKS**

CARD NO.

Expiration date *Signature*

④ Send your order to:
AEE BOOKS
P.O. Box 1026
Lilburn, GA 30048

INTERNET ORDERING
www.aeecenter.org/books
(use discount code)

TO ORDER BY PHONE
Use your credit card and call:
(770) 925-9558

TO ORDER BY FAX
Complete and Fax to:
(770) 381-9865

INTERNATIONAL ORDERS
Must be prepaid in U.S. dollars and must include an additional charge of $10.00 per book plus 15% for shipping and handling by surface mail.

$$V_{PCC} = k \cdot \sqrt{\left(V_{MEA} - R_{ccT} \cdot I_{dMEA} + X_{ccT} \cdot I_{qMEA}\right)^2 + \left(X_{ccT} \cdot I_{dMEA} + R_{ccT} \cdot I_{qMEA}\right)^2}$$

The real power at the PCC P_{PCC} can be computed stating from the real power measured at the 270 V side of the transformer P_{MEA} as:

$$P_{PCC} = P_{MEA} - R_{ccT} \bullet (I^2_{dMEA} + I^2_{qMEA}) - P_0$$

Where:

k: nominal voltage ratio of the boost transformer 400/270 V,

R*ccT*: equivalent series resistance of the boost transformer at the 270 V side,

X*ccT*: equivalent series reactance of the boost transformer at the 270 V side,

I*dMEA*: current on the d-axis measured at the 270 V side of the transformer,

I*qMEA*: current on the q-axis measured at the 270 V side of the transformer.

Two relevant aspects related to the exploitation of the inverter for the modulation of the reactive power have to be considered: a) to ensure a suitable voltage level at the DC-Link in all operating conditions and b) the increase of the inverter losses during the reactive power modulation.
In the following sections these aspects are discussed.

DC-Link Voltage Level

The presence of a primary source during the daytime combined with the inverter operation ensures the required DC voltage control to achieve proper operation and harmonic free output-current. However, during the night-time the primary source is not available. Supposing to manage PV generators as reactive power sources also in these conditions, it is required a dedicated strategy to address the need for proper DC-Link voltage control.

During inverter operation, when the primary source is not available, DC bus voltage control (function 2.) is required not only to ensure proper modulation patterns but also to achieve a "harmonic-free" reactive current. The DC-Link voltage will also meet the following conditions:

a) $V_{DC\text{-}Link} \mid \min > V_{ac} \mid pk$

b) $V_{DC\text{-}Link} \mid \max < V_{PV} \mid$ reverse bias

The first condition will prevent uncontrolled current flow from the grid back to the DC bus capacitors through the freewheeling diodes integrated to the inverter power switches and hence the potential risk of damage to these diodes (which is not able to withstand large inrush currents). The second condition will be met to prevent back-feeding the PV array with a large and uncontrolled reverse current.

In the case when the DC power is not available ($V_{DC\text{-}Link} < V_{ac}|pk$), the equivalent circuit of an inverter is a bridge rectifier, but the IGBT's freewheeling diodes are not able to withstand the high inrush current produced during uncontrolled charging of the DC bus capacitors. Under these conditions, extending inverter operation over the full-time period imposes the addition of an ancillary circuit for the activation of a suitable pre-charge function (function 3). This circuit is activated when the inverter is disconnected from the grid; the ancillary circuit will provide the proper amount of energy for restoring and maintaining suitable DC-Link voltage level for the necessary amount of time required by the inverter to emulate a synchronous version of the AC voltage ensuring a smooth re-closure of the AC contactor in the case of trip off-line.

Inverter System Losses

The reactive power modulation achieved by the inverter increases the lagging/leading current flow along the valves of the converter. The impact of the higher current flow with respect to the unitary power factor operation condition has to be taken into account in terms of losses deterioration and ageing of the apparatus. Fig. 7 shows the scheme of one phase of the inverter.

Fig. 8 shows the voltages and currents behaviour over time during a phase modulation. In particular, the first graph reports the AC current output $i_1(t)$, the AC voltage output $v_1(t)$ and the fundamental voltage $v_{1(1)}(t)$ at the AC side; the second graph reports the IGBT current and the third the diode current [30].

The phase shift between the voltage and the fundamental harmonics of the AC current is described by the φ angle, as indicated in the first graph of the Fig. 8. For a given real power value, the inverter has to inject a current with higher rms value so as to inject reactive power with respect to a unitary power factor operation condition. Higher is the φ angle, higher is the current i_{F2} flowing in the freewheeling diodes (third graph of Fig. 8), therefore the $\cos\varphi$ determines how the total power dissipation is divided between the IGBT and diode. Furthermore, the diode losses are higher

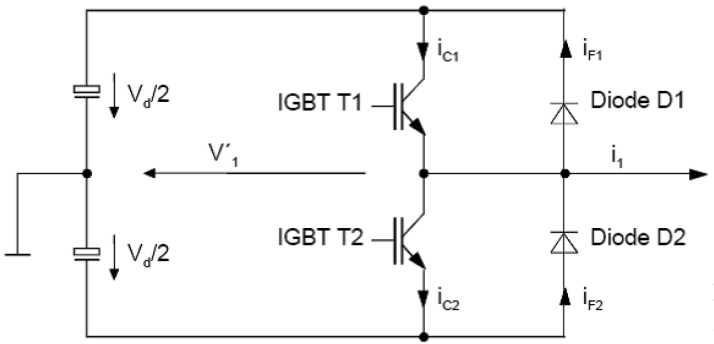

Fig. 7: Converter phase (source [29])

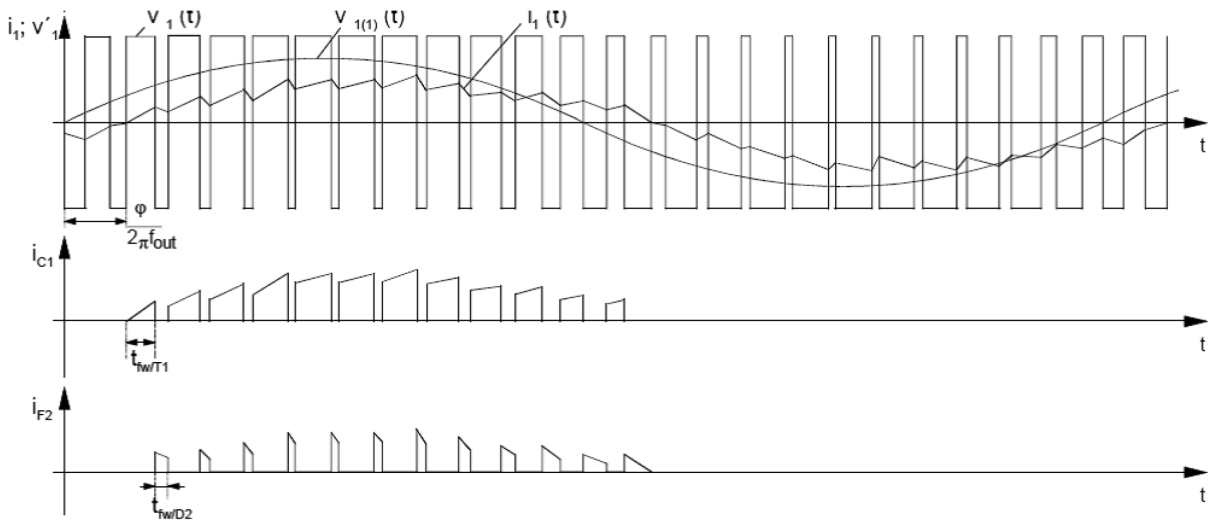

Fig. 8: AC voltage and current output, IGBT and diode current during a phase modulation (source [29])

than the IGBT because of the higher resistance of the former component therefore higher is the φ angle higher is the total losses of the converter.

NUMERICAL ANALYSIS

Numerical analyses are carried out in order to evaluate the impact of the local voltage control strategies on the LV distribution system and effect on the inverter system in response to the reactive power modulation.

Analysis Impact on the Distribution System—Network Model

The impact of the proposed voltage regulation strategies on the LV distribution system is evaluated by carrying out some numerical analyses. A model based on MATLAB-Simulink/SimPowerSystem software is built. The goal of the numerical analysis is to estimate the benefit given by the reactive power modulation on the voltage profile of an LV distribution feeder. The study case network is the radial LV feeder reported in Fig. 9. The system corresponds to the scheme adopted for the experimental analysis.

Three PV inverters have been modelled: INV1 and INV2 (20 kW rated power) managed according to the four control laws, and INV3 (30 kW rated power) representing a generic (variable) load. The impedance values $Z_{Network}$, $Z_{cable\ 4G16}$ and Z_{TL} are defined in order to obtain the equivalent series impedance $Z_{TOT} = 0.59 + j0.32\ \Omega$. This value is equal to the maximum reference impedance value for the 95% of LV customers in Italy [16]. This value was chosen to the maximum so as to have a weak network.

Since the system has a stable behaviour at high frequency, the further numerical simulations are carried out exploiting a simplified model at the fundamental frequency of 50 Hz (i.e. a low frequency model without considering the ripple of switching). A low frequency model of the inverter is considered appropriate to model the reactive power modulation and the real power curtailment strategies, which are regulation actions with a lower time constant than the switching commutation period.

In the low frequency model the three-phase inverter is modelled as three controlled AC voltage sources on the AC side and a controlled DC current source on the DC side according to the mathematical model reported in the following equations:

$$\begin{cases} v_A = h_A \cdot V_{DC} \\ v_B = h_B \cdot V_{DC} \\ v_C = h_C \cdot V_{DC} \\ i_{DC} = -(h_A i_A + h_B i_B + h_C i_C) \end{cases}$$

where h_A, h_B and h_C are the switching functions of each phase of the inverter; they are the output mathematical functions of the voltage control of the inverter expressed in per unit. This simplified model lets the computational complexity of the simulations be strongly reduced; therefore, it is possible to run simulations longer. The block diagram adopted to model the three-phase inverter for the following numerical simulations is reported in Fig. 10.

In order to evaluate the performances of the proposed voltage control law, a one-year analysis is carried out. The inverter INV3 is adopted as cumulative load connected at the end of the LV feeder; the daily average curves adopted are calculated by exploiting measurements on LV passive customers [26]. These average curves have been rescaled with respect to the rated value of 30 kW, furthermore, a random noise with null average is added in order to obtain a stochastic load model. Inverters INV1 and INV2 inject power according to the average daily curves of a 20 kW photovoltaic power plant; these data are based on real measurements available in [27].

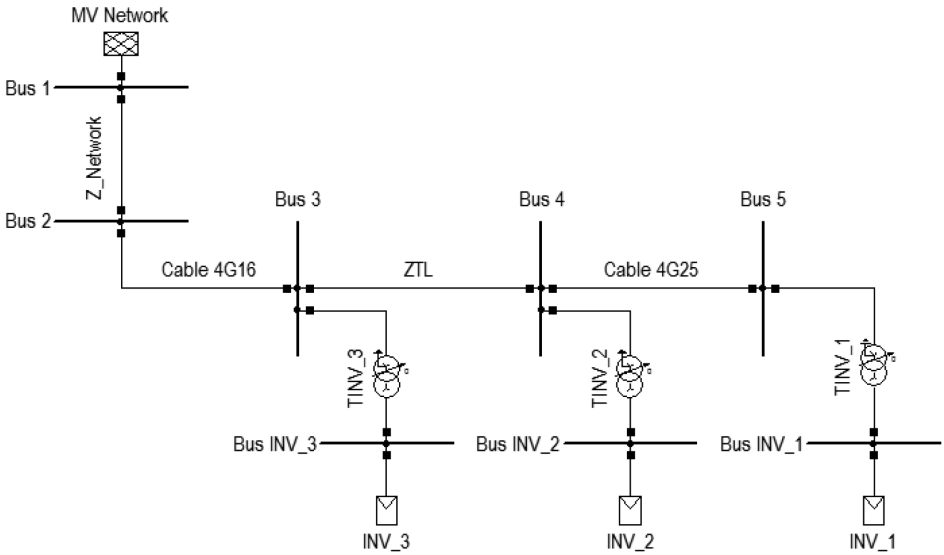

Fig. 9: Testing feeder

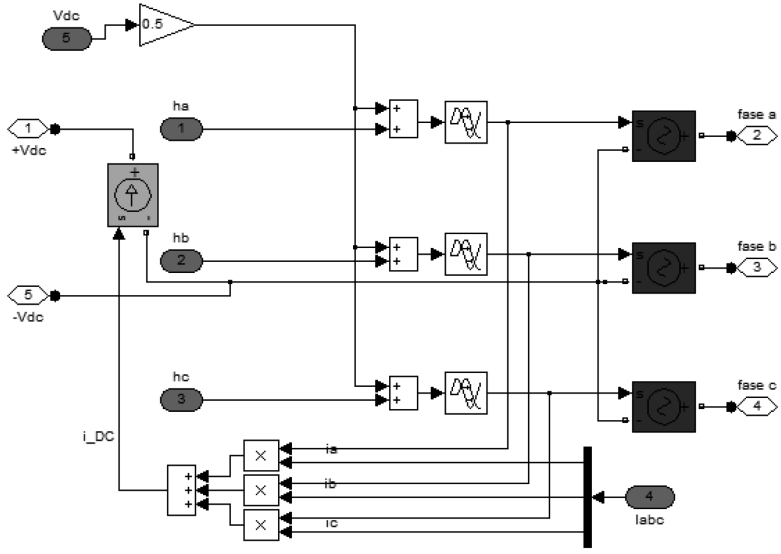

Fig. 10: Model of a three-phase inverter for 50 Hz frequency simulations

For these curves a random function with null average is added in order to simulate the effect of the weather trend in the photovoltaic production.

Analysis Impact on the Distribution System—Numerical Simulation Results

The performances of the proposed local characteristics are analysed by evaluating the voltage profile enhancement, the Hosting Capacity (HC) and real energy losses over the one-year chronological analysis.

First, the HC index is computed. The approaches proposed in the literature were typically based on an iterative DG penetration increase in a given bus, until operating limits were violated (nodal HC) [12][13]. In this paper, the HC computation has been extended to more than one DG injection considered at the same time. Furthermore, the HC computation has been extended considering a one-year period. In Table 1 the HC results are reported; the annual multi-generator HC index is evaluated according to the overvoltage limit of +10% of the rated voltage (EN 50160 prescriptions). The results are the maximum real power that can be injected simultaneously by each of the two inverters INV1 and INV2 all over the year without voltage violations. The HC results show that for a unitary power factor operation condition (first line of the table), the feeder can host only two power plants of 12.5 kW and the adoption of the reactive power con-

trol laws allows increasing the HC of the system.

Control laws A and B, in which the reactive modulation is computed as a function of the PCC voltage, are the most effective in terms of HC with respect to the Law C and Law D (linked to the real power injections). In order to further increase the HC (i.e. higher integration of renewable energy sources in the grid) the control strategy requires a limitation of the real power injected at the PCC. For this purpose, the real power curtailment strategies DG disconnection and DG limitation, described in section 0, are tested. Furthermore, the combination of local voltage control and real power curtailment is tested.

A scenario of power injections equal to 20 kW (for both INV1 and INV2) is considered, thus exceeding the HC of the feeder (see Table 1). On the basis of this hypothesis, the performance of the regulation strategies are evaluated with regard to the following two indices:

- $\Delta E_{prod-PV}$ [kWh]: annual energy production of the DG unit w.r.t. the reference value of 44136 kWh/year which is equal to the case of unitary power factor operation of the PV plant and without any disconnection if over-voltages occur ("Ideal scenario");

- $\Delta E_{Grid-Loss}$ [kWh]: annual energy losses in the grid with respect to the reference value of 3428 kWh/year which is computed in the Ideal scenario.

Table 2 reports the value of the indices above defined for the one-year analysis. It can be concluded that the DG limitation strongly reduces the energy curtailment with respect to the DG disconnection. In addition, a combination of reactive power modulation and real power curtailment can further reduce the energy curtailment in order to re-establish the voltage within the limits. Looking at $\Delta_{Eprod-PV}$ values, the control Law B (included in the CEI 0-21) seems to be the most effective control strategy because it is possible to minimize the DG production curtailment (0.08% of lack of energy production with respect to the ideal scenario if the DG limitation strategy is adopted). Anyway, for Law B the energy loss deterioration is the highest (+9.5%) and the global energy available has to be computed in order to evaluate the total benefit of the system.

In Table 3 the global benefit of the system is evaluated; in particular, the increase in the energy production ($\Delta E'_{prod\_PV}$) and the increase in the network losses ($\Delta E'_{Grid\_Loss}$) are computed both **with respect to the uni-**

Table 1: Annual multi-generator hc (p_{dg} of INV1 and INV2) with load INV3

	HC [kW]	ΔHC [%]
cosϕ=1	12.5	-
Law A	14.5	+16.0%
Law B	14.8	+18.4%
Law C	13.3	+6.4%
Law D	13.3	+6.4%

Table 2: Simulation results adopting the real power curtailment strategies combined with the voltage control laws at PDG = 20 kW

	DG disconnection		DG limitation	
	ΔE_{prod_PV} [KWh]	ΔE_{Grid_Loss} [kWh]	ΔE_{prod_PV} [KWh]	ΔE_{Grid_Loss} [kWh]
cosϕ=1	-3226 (-7.31%)	-463 (-13.5%)	-318 (-0.72%)	-48 (-1.39%)
Law A	-1046 (-2.37%)	-180 (-5.2%)	-88 (-0.20%)	+149 (+4.34%)
Law B	-504 (-1.14%)	+136 (+3.9%)	-35 (-0.08%)	+326 (+9.51%)
Law C	-2665 (-6.04%)	-424 (-12.4%)	-225 (-0.51%)	-21 (-0.61%)
Law D	-2224 (-5.54%)	-381 (-11.1%)	-269 (-0.61%)	-32 (-0.93%)

tary power factor operation condition. Furthermore, the energy available at the Secondary Substation (ΔE_{SS}) is computed as the difference between $\Delta E'_{prod\_PV}$ and $\Delta E'_{Grid\_Loss}$. By adopting Law B the index ΔE_{ss} is negative, it means that this strategy does not introduce a global benefit for the system because the increasing in the network losses is higher than the increase in energy production. It can be concluded that Law C (mentioned in CEI 0-21) has the highest global energy benefit resulting in a 66 kWh of energy available for the SS (third column of Table 3).

The analysis carried out for the different control laws shows that it is possible to mitigate the over-voltages in the LV distribution network and partially improve the HC by exploiting DG unit as reactive power resources decentralized along the distribution system. As long as the R/X ratio of the LV testing feeder is high, the real power curtailment results to

Table 3: Changing in the energy production and losses with respect to the unitary power factor condition in the case of dg limitation combined with reactive power modulation

	$\Delta E'_{prod\_PV}$ [kWh]	$\Delta E'_{Grid\_Loss}$ [kWh]	ΔE_{SS} [kWh]
Law A	+230	+197	+33
Law B	+283	+374	-91
Law C	+93	+27	+66
Law D	+49	+16	+33

be effective in the voltage quality enhancement with only a slight lack of DG production.

These numerical results highlight the performances of the local control strategies in the voltage regulation. In the next paragraphs, the experimental campaign is described to test the implementation feasibility of the control laws in the inverter control algorithm and the stability of the network in the case of step-stress injection of real power in a multi-generation scenario.

Analysis of the Inverter System in Response to the Reactive Power Modulation

The analysis discussed in the previous paragraphs describes the benefit of the reactive power modulation for the distribution system; in particular, the contribution of the four local control laws in the voltage profile enhancement is evaluated.

In this section, the deterioration of the converter efficiency during the reactive power modulation is analysed. The inverter losses are computed according to the method reported in [28] starting from inverter system data (inverter and transformer). The losses results of a 20 kW three-phase inverter (i.e. the same rated power assumed in the previous section) are reported in Table 4 for both unitary power factor ($\cos\varphi = 1$) and 0.9 lagging power factor ($\cos\varphi = 0.9$) operation conditions (column $\cos\phi$ of the table). Different real power loadings are considered (from 5% to 100% of the inverter rated power). The table discerns the losses due to the IGBT and the one of the free-wheeling diodes of the apparatus. The reported

Table 4: IGBT and diode losses [W] for different cosϕ values and loading for a 20 kW inverter system

	cosφ	5%	10%	20%	30%	50%	75%	100%
IGBT forward power dissipation	1	0.351	0.487	0.869	1.291	2.189	3.394	4.698
	0.9	0.386	0.572	1.046	1.551	2.600	3.966	5.406
Diode forward power dissipation	1	0.829	1.413	2.735	4.165	7.279	11.617	16.431
	0.9	0.866	1.508	2.962	4.547	8.043	12.994	18.569
IGBT switching power dissipation	1	2.509	4.023	7.360	10.789	17.718	26.437	35.199
	0.9	2.656	4.388	8.136	11,963	19.684	29.398	39.163
Diode switching power dissipation	1	0.673	1.079	1.975	2.894	4.754	7.093	9.444
	0.9	0.713	1.177	2.183	3.210	5.281	7.887	10.507
IGBT total power dissipation	1	2.860	4.510	8.229	12.080	19.906	29.831	39.897
	0.9	3.042	4.960	9.181	13.514	22.283	33.364	44.569
Diode total power dissipation	1	1.502	2.492	4.709	7.059	12.033	18.710	25.874
	0.9	0.713	1.177	2.183	3.210	5.281	7.887	10.507
Total IGBT+Diode dissipation	1	4.362	7.002	12.938	19.139	31.939	48.541	65.771
	0.9	4.620	7.645	14.326	21.270	35.607	54.245	73.645
Inverter total power dissipation	1	**26.174**	**42.012**	**77.630**	**114.834**	**191.634**	**291.247**	**394.627**
	0.9	**27.722**	**45.871**	**85.956**	**127.622**	**213.642**	**325.470**	**441.871**

values are related to a single valve whilst the row "Inverter total power dissipation" points out the total losses of the six IGBT and the six diodes of the three-phase inverter.

The remaining losses of the inverter system are due to the components such as transformer, capacitor filters and reactance filters. These losses are reported in Table 5; both unitary power factor (cosφ = 1) and 0.9 lagging power factor (cosφ = 0.9) operation conditions are considered for different real power loading values.

The total losses of the converter are reported in Table 6; these values are computed by adding together, for each condition, the IGBT and valve (Table 4) and the filter and transformer losses (Table 5). In Table 7 the ef-

Table 5: Transformer and filters losses of a 20 kW inverter system

	cosφ	5%	10%	20%	30%	50%	75%	100%
Inverter output power [kW]	-	1	2	4	6	10	15	20
Inverter output current [A]	1	1.4	2.9	5.8	8.7	14.4	21.7	28.9
	0.9	1.6	3.2	6.4	9.6	16.0	24.1	32.1
Magnetic losses of the transformer [W]	1	120	120	120	120	120	120	120
	0.9	120	120	120	120	120	120	120
Joule losses of the transformer [W]	1	1	2	9	20	56	125	222
	0.9	1	3	11	25	69	154	274
Total losses of the transformer [W]	1	121	122	129	140	176	245	342
	0.9	121	123	131	145	189	274	394
Losses of the C filter bank [W]	1	0.17	0.17	0.17	0.17	0.17	0.17	0.17
	0.9	0.17	0.17	0.17	0.17	0.17	0.17	0.17
Losses of the L filter [W]	1	0.6	1.6	5.6	12.2	33.3	74.5	132.2
	0.9	0.6	1.6	5.6	12.2	33.3	74.5	132.2
Voltage drop of the L filter [V]	1	0.4	0.6	1.1	1.6	2.6	3.9	5.2
	0.9	0.4	0.6	1.2	1.7	2.9	4.3	5.8
Reactive power of the L filter [Var]	1	3.2	8.2	28.2	61.5	168.0	376.1	667.3
	0.9	3.6	9.8	34.4	75.5	207.1	463.9	823.5
Total losses for filter and transformer [W]	1	**121.4**	**124.0**	**134.6**	**152.4**	**209.0**	**319.7**	**474.6**
	0.9	**121.4**	**124.5**	**136.7**	**157.0**	**222.0**	**349.0**	**526.7**

Table 6: Total losses [W] of a 20 kW inverter system

	cosφ	5%	10%	20%	30%	50%	75%	100%
Inverter total power dissipation	1	26.2	42.0	77.63	114.8	191.6	291.3	394.6
	0.9	27.7	45.9	85.9	127.6	213.6	325.5	441.9
Total losses for filter and transformer	1	121.4	124.0	134.6	152.4	209.0	319.7	474.6
	0.9	121.4	124.5	136.7	157.0	222.0	349.0	526.7
Total losses for the converter	1	**147.5**	**166.0**	**212.3**	**267.2**	**400.6**	**610.9**	**869.2**
	0.9	**149.2**	**170.4**	**222.6**	**284.6**	**435.6**	**674.4**	**968.6**

ficiency computed by exploiting the total losses of Table 6 is reported as a function of the real power injected. The comparison between the unitary power factor operation condition and the reactive power modulation condition at cosϕ = 0.9 is presented.

In the case of reactive power modulation the losses are higher and the efficiency is lower than the unitary power factor operation. The increase in losses is caused by the two aspects explained below.

- Increasing of the forward and switching power dissipation of the inverter, caused by the shifting between the AC voltage and the AC current phasors (as described in Table 4).

- Increasing of the rms value of the inverter AC current due to the reactive component that introduces higher losses in the filter inductance and in the transformer.

On the contrary, the power losses on the capacitance filter and the magnetic losses of the transformer are independent of the higher RMS current value.

The last row of Table 7 reports the increase in the inverter losses by switching from cosφ = 1 to cosφ = 0.9 and keeping the real power injection fixed. They are the part of losses given by the reactive current component. At 100% power output (20 kW) the losses contribution due to the lagging current component are almost 12% of the losses at unitary power factor.

The analyses carried out depict that, the small reduction in the power efficiency at cosφ = 0.9 (from 95.84% to 95.38% at 100% power output) and the corresponding small losses increase can be considered negligible and they are not an inconvenience for the implementation of the voltage control strategies in already existing inverters.

Nevertheless, it is recommended to fit the thermal sizing of the inverter for a forward-looking application of the voltage control; the heat sink and the ventilation system have to guarantee the correct operation of the converter in the case of reactive power modulation and they have to be able to dissolve the higher power losses in order not to compromise the lifetime and the reliability of the equipment. From an economic point of view, the main additional costs are the pre-charge circuit and the sensors required to control the DC-Link voltage; they are not considerable costs.

In conclusion, the benefit in terms of voltage quality enhancement introduced by the local control laws cannot be compared to minor drawbacks in terms of losses deterioration due to a higher current flow in the inverter system.

Table 7: Efficiency of the converter system [%] for cosφ = 1 and cosφ = 0.9 operation condition and different real power outputs

	5%	10%	20%	30%	50%	75%	100%
cosφ = 1	87.14	92.33	94.96	95.74	96.15	96.09	95.84
cosφ = 0.9	87.02	92.15	94.73	95.47	95.83	95.70	95.38
Inverter system losses increase	1.098	2.603	4.878	6.522	8.735	10.40	11.43